JOURNAL OF MATERIALS SCIENCE 9 (1974) 1446–1455

Complex alloy powders produced by different atomization techniques: relationship between heat flow and structure

P. A. JOLY, R. MEHRABIAN
Department of Metallurgy and Materials Science, Massachusetts Institute of Technology, Cambridge, Massachusetts, USA

Pre-alloyed powders of Maraging 300, IN-100, and MAR-M-509 alloys made by different atomization techniques are compared with respect to chemistry, size, morphology and microstructure. Depending on the process employed and on the size and morphology of the powders produced, measured oxygen contents and secondary dendrite arm spacings vary from 40 ppm to 2000 ppm and 2 to 12 μm, respectively. For the Maraging 300 alloy the relationship $d = 39.8\epsilon^{-0.30}$ between secondary dendrite arm spacing, d, and local average cooling rate, ϵ, is established. A simple heat flow analysis is presented which permits calculation of heat-transfer coefficients and solidification times of powders using this relationship. For example, a heat-transfer coefficient $h = 3.9 \times 10^{-3}$ cal cm^{-2} sec^{-1} °C^{-1} is calculated during solidification of steam atomized coarse powders of Maraging 300 alloy.

1. Introduction

The two important structural parameters influencing properties of components made by direct casting or via atomization are grain size and dendrite arm spacing. While fine grain size generally improves room temperature properties, large grains, sometimes with specified orientations are preferred in high temperature applications. On the other hand, the dendritic structure within the cast grains has as great, or greater, influence on properties at all temperatures. Regions between dendrite arms are usually rich in solute, contain equilibrium and/or non-equilibrium second phases and microporosity. With decreasing dendrite arm spacings homogenization of solute segregation becomes commercially feasible, and second phases (inclusions and microporosity) become finer and more evenly distributed. Experimental evidence available for a variety of cast alloys indicates that dendrite arm spacing is influenced only by local average cooling rate or "local solidification time".* Thus, refinement of dendritic structure by increasing the rate of heat extraction during solidification of castings has become of foremost importance in solidification technology.

The most important common advantage of parts produced by compaction of atomized powders over parts directly cast to shape is the fine dendritic structures of the powders. New atomization techniques developed in the past decade are currently being applied to production of high strength, highly alloyed materials. Whether the powder metallurgy route will succeed in replacing the casting and ingot approach, in these more complex alloys, depends on the chemical integrity of the powders which influences their subsequent successful consolidation into fully dense, heat-treatable parts.

The aim of this investigation was to: (1) study the relationship between rate of heat extraction during solidification and structures of atomized powders, and (2) compare the structural features and chemical integrity of highly alloyed materials cast by different atomization processes. The three alloys studied were iron base Maraging 300 alloy,

*"Local solidification time" is defined as time at a given location in a casting between initiation and completion (or near completion) of solidification. It is inversely proportional to local average cooling rate at that location.

nickel base IN-100 alloy, and cobalt base MAR-M-509 alloy. In lieu of direct experimental temperature measurements during solidification of atomized powders, solidification times versus powder particle size are calculated using heat flow expressions coupled with an experimental relationship developed between local average cooling rates and secondary dendrite arm spacings of Maraging 300 alloy. Pre-alloyed powders of the three alloys produced by steam, inert gas, vacuum (soluble gas), rotating electrode, and spin atomization are compared with respect to their chemistry, size, morphology and segregate spacings.

2. Experimental procedure

2.1. Maraging 300 alloy cast at different cooling rates

The effect of a range of cooling rates, 0.1 to 10^3 °C sec^{-1}, on the secondary dendrite arm spacings of Maraging 300 alloy was determined. The various cooling rates were obtained by levitation-melting and casting of small droplets (1 to 2 g), unidirectional solidification of a 2.5 kg ingot, and vacuum-melting of a 700 g charge in an alumina crucible and furnace-cooling.

2.1.1. Levitation-melting and casting

Fig. 1 is a sketch of the levitation-melter and associated apparatus. The details of this apparatus have previously been described [1]. Droplets of the Maraging 300 alloy were levitated inside the glass tube in an atmosphere of helium. The temperature of the droplets was continuously monitored using a two-colour optical pyrometer. The molten levitated droplets were solidified and cooling rates measured using the following techniques.

(a) *Gas-quenching.* With sufficiently high flow rates of hydrogen or helium, droplets were solidified while levitated. Measured cooling rates, via the two-colour optical pyrometer, were of the order of 1 to 15°C sec^{-1}.

(b) *Oil-quenching.* A somewhat higher cooling rate was obtained by liquid-quenching. The liquid quench tank was placed below the exit port shown in Fig. 1; the power to the levitation coil was turned off, and the charge dropped through the plastic seal into the liquid. A cooling rate of $\sim$ 140°C sec^{-1} has previously been calculated for oil quenching [2].

(c) *Chill casting.* Chill castings in a copper mould with plate-shaped mould cavity of 2 mm thickness, inserted in the turntable in the enclosure in Fig. 1, were made and cooling rates on the order of 10^3 °C sec^{-1} were measured as previously described [1].

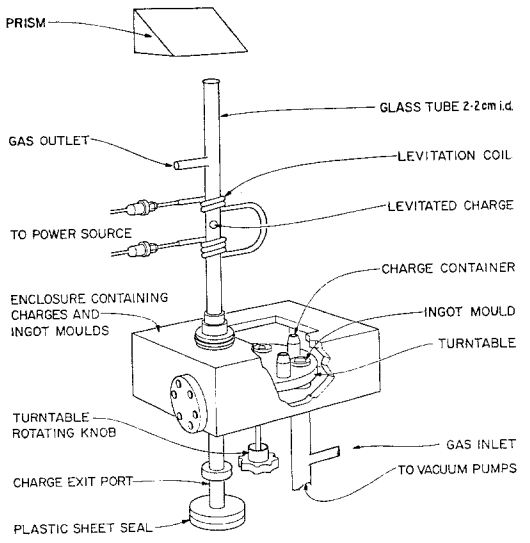

Figure 1 Sketch of levitation melting and casting apparatus.

2.1.2. Unidirectional casting

A 5 cm × 5 cm × 7.5 cm tall unidirectional ingot of the Maraging 300 alloy was cast using a composite mould of CO_2 sand and insulating moulding material, Fiberchrome. A water-cooled stainless steel chill was located at the base opening of the mould. Thermal measurements were made by utilization of four Pt/Pt-10% Rh silica-shielded thermocouples located along the length of the ingot mould.

2.1.3. Vacuum-melting and furnace-cooling

Several specimens of Maraging 300 alloy weighing approximately 700 g were vacuum-melted in an alumina crucible. These samples were solidified inside the crucible by decreasing the power input to the furnace at different rates and temperature profiles were recorded with a Pt/Pt-10% Rh thermocouple inserted in the melt.

2.2. Atomization processes

Pre-alloyed vacuum-cast ingots of Maraging 300, IN-100 and MAR-M-509 alloys were sent to different commercial establishments for atomization. The powders were made by:

(a) *Inert gas atomization.* The pre-alloyed

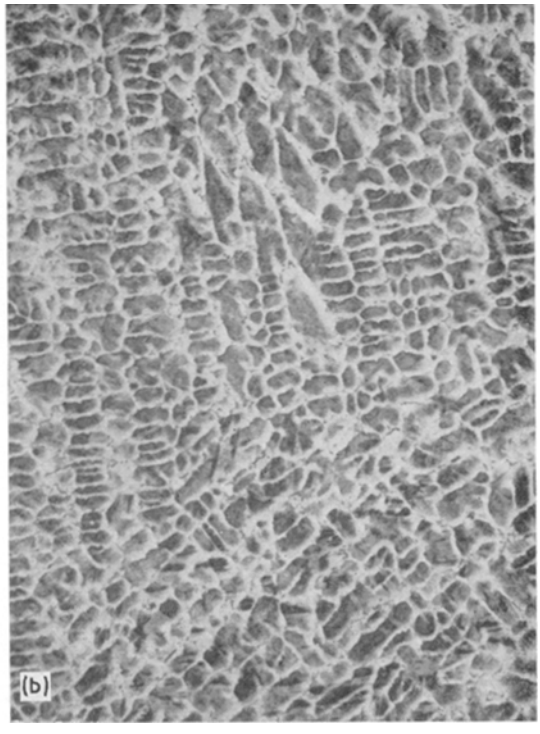

Figure 2 Variation of microstructure with cooling rate for Maraging 300 alloy. (a) Gas quench, (b) liquid quench, (c) chill cast. × 188.

ingot is vacuum-remelted and atomized by a stream of high purity argon gas.

(b) *Rotating electrode process.* The end of a consumable rotating electrode of the alloy is arc-melted in an inert atmosphere and fine droplets are flung off by centrifugal force.

(c) *Spin atomization.* A new proprietory process where atomization is achieved by pressurizing the whole melt as opposed to disintegration of a liquid metal stream by a quenching medium.

(d) *Steam atomization.* The pre-alloyed ingot is remelted in an atmosphere and atomized by a stream of low-pressure steam.

(e) *Vacuum atomization.* The remelted alloy is pressurized and saturated with hydrogen. Atomization is obtained through a "pressure nozzle" operating between the hydrogen-filled chamber and a vacuum chamber.

Powder particles of the three alloys, made by the different processes listed above, were analysed by routine chemical and vacuum fusion techniques. The powders were also characterized by morphology and size distribution. Finally, standard optical metallographic and SEM techniques were used to study internal and surface structures of the powders.

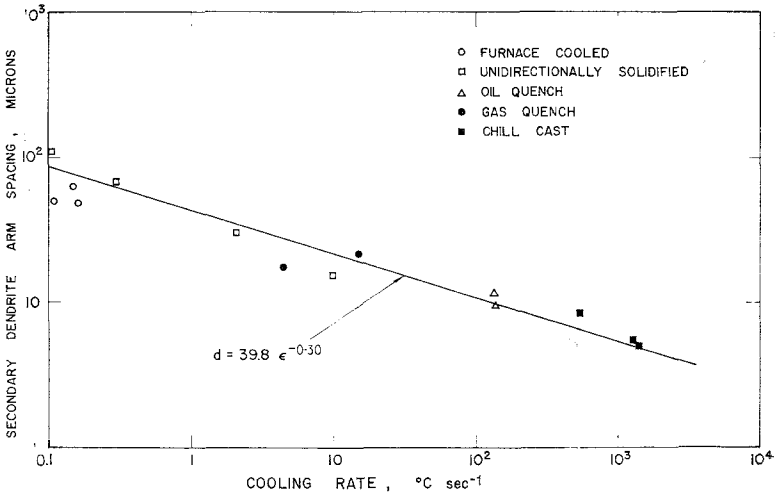

Figure 3 Secondary dendrite arm spacing versus cooling rate in Maraging 300 alloy.

3. Results and discussion

3.1. Dendrite arm spacing versus cooling rate

The effect of cooling rate during solidification on secondary dendrite arm spacings of Maraging 300 alloy is shown in Figs. 2 and 3. Generally, for a wide variety of cast alloys, dendrite arm spacing is found to be inversely proportional to local average cooling rate to an exponent (or directly proportional to "local solidification time" to the same exponent) [1, 3, 4]. The relationship for a given alloy is:

$$d = at_f^n = b(\epsilon)^{-n}, \quad (1)$$

where d is secondary dendrite arm spacing, a and b are constants, t_f is "local solidification time", ϵ is local average cooling rate, and the exponent, n, is usually in the range of $\frac{1}{3}$ to $\frac{1}{2}$.

Fig. 2 shows how the microstructure of the Maraging 300 alloy is refined by increasing the local average cooling rate during solidification. Fig. 3 is a plot of the secondary dendrite arm spacings versus local average cooling rates on a log-log plot. The exponent, n, in Equation 1 determined for this alloy is 0.30.

3.2. Evaluation of atomized powders

Powders of the three alloys processed by different atomization techniques were characterized by chemical purity, morphology, size, and secondary dendrite arm spacings. Results of this study are presented in Table I and Figs. 4 to 6. Examination of these data permits the following observations.

3.2.1. Gas contents

Powders of all three alloys made by rotating electrode process, spin- or vacuum-atomization processes have oxygen contents less than 100 ppm. The argon-atomized fine powder is slightly higher in oxygen content at 170 ppm. It appears that spin-atomized powders are the cleanest with respect to argon, nitrogen and hydrogen contents, while, as expected, steam atomization resulted in the highest oxygen and nitrogen contents.

3.2.2. Powder size and morphology

Both the rotating electrode process and spin-atomized powders were spherical in shape and had relatively narrow size ranges. For example, in the spin-atomized Maraging 300 alloy, median particles size $\sim$ 430 μm, 68% by weight of the particles were in the 370 to 490 μm size range. Fig. 4 shows scanning electron micrograph views and a photomicrograph of a polished and etched cross-section of spin-atomized Maraging 300 alloy powder. The same type of smooth, well rounded, and uniform powder particles were also obtained in the IN-100 and MAR-M-509 alloys.

The vacuum-atomization process, while leading to production of clean powders (Table I) has little control over powder shape. The powders consist of spheres and flakes. The inert gas atomized powders are generally spherical in shape with finer particles attached to coarser particles. Fig. 5 compares scanning electron micrograph views of representative powder

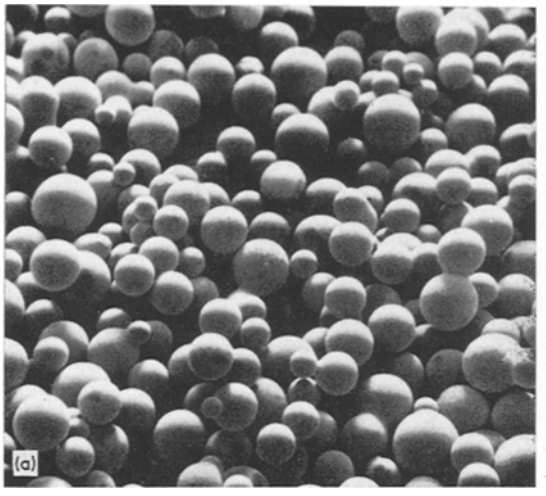

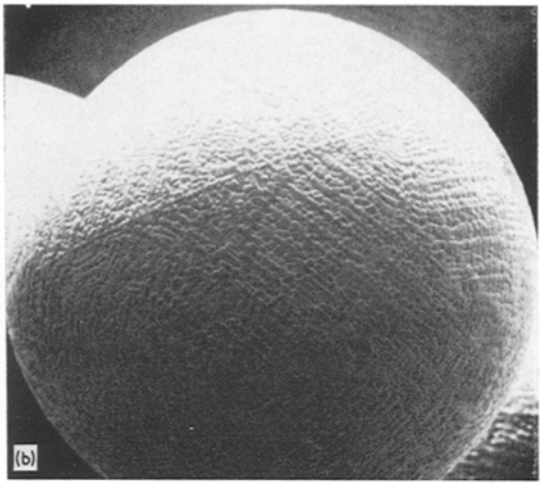

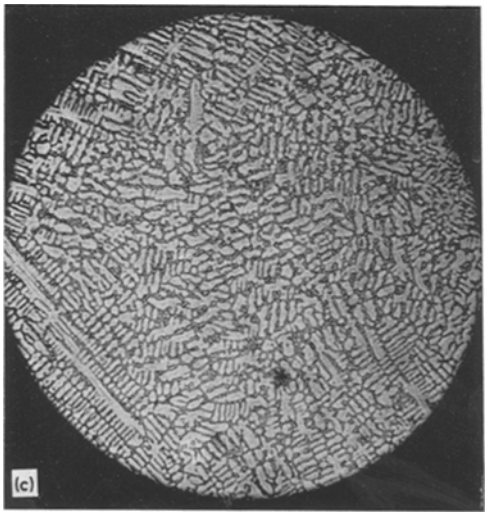

Figure 4 Spin-atomized powders of Maraging 300 alloy; (a) and (b) are SEM micrograph views at × 14 and ×177, respectively, (c) is a photomicrograph of a polished and etched cross-section at × 147.

particles of IN-100 alloy produced by spin-, vacuum- and inert gas atomization processes.

Steam atomization produces coarse, spherical particles, with some included porosity, in Maraging 300 alloy. However, it is not a suitable process for MAR-M-509 and IN-100 alloys. The powders of the latter two alloys are hollow spheres and flakes and thin sharp flakes, respectively. The flakiness of the powders is caused by the high surface oxidation of the broken liquid streams preventing their subsequent spheroidization by surface tension forces.

3.2.3. Dendrite arm spacing

Table I lists the range of measured secondary dendrite arm spacings of the three alloys produced by the different atomization techniques. Fig. 6 is a plot of the measured secondary dendrite arm spacings of the Maraging 300 alloy versus diameter of the spherical powders. As expected, local average cooling rate, and hence measured secondary dendrite arm spacing, is influenced primarily by the size of the particles, and to a lesser extent the coolant environment employed. For example, average secondary dendrite arm spacings in spin- and vacuum-atomized Maraging 300 alloy powders is 4.0 to 7.0 μm, and in coarse powders made by steam or argon atomization, it is 4.5 to 12 μm (see Table I for powder particle sizes). The corresponding cooling rates, from Fig. 3, are 3.3×10^2 to 2.1×10^3 °C sec^{-1} for the vacuum- and spin-atomized powders and 54 to 1.4×10^3 °C sec^{-1} for the coarse argon- and steam-atomized powders.

3.3. Heat flow during atomization

During solidification of small spherical alloy droplets, heat flow is controlled by both convection at the surface and by radiation. However, there are no known values for the combined radiative and convective heat transfer coefficient, and direct measurement of the cooling rate or the heat flux during solidification of an atomized droplet is extremely difficult, if not impossible.

The following discussion shows a method for computing the cooling rate, then the heat-transfer coefficient, and finally the solidification time of an atomized droplet. Using Newton's

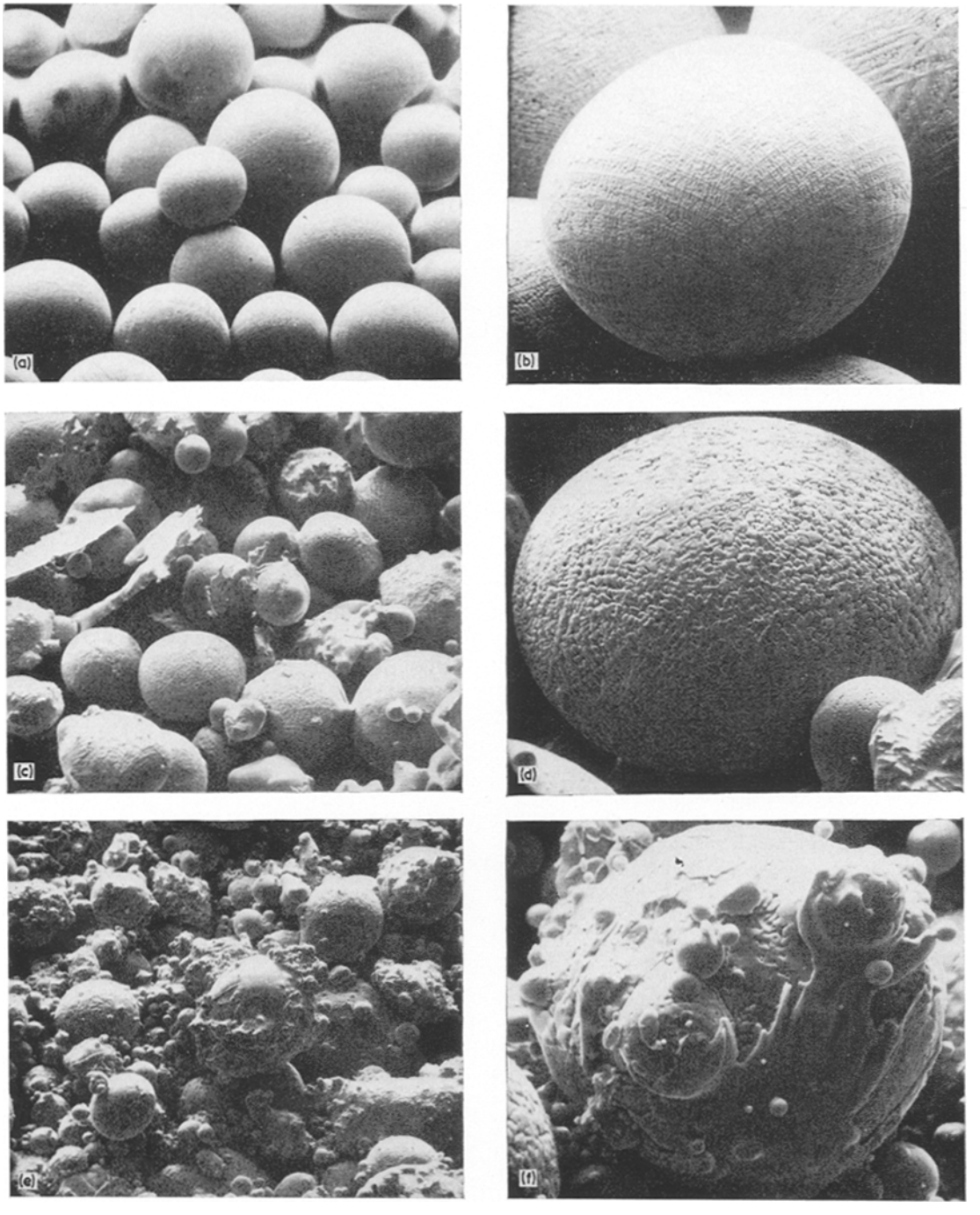

Figure 5 SEM views of atomized powders of IN–100 alloy; (a) and (b) show spin-atomized powders at × 40 and × 155, respectively; (c) and (d) show soluble gas (hydrogen)-atomized powders in vacuum at × 41 and × 163, respectively; (e) and (f) show inert gas-atomized powders at × 152 and × 780, respectively.

law of cooling, coupled with an overall heat balance, Equations A1 and A2 in the Appendix respectively, an expression for volume fraction of the droplet solidified versus time is obtained:

$$g_s = Bt \qquad (2)$$

TABLE I Powder descriptions

Atomization process	Median size (μm)	Dendritic arm spacing range (μm)	Gas content (ppm) O	N	H	Ar	Shape of powders
Cobalt base alloy MAR-M-509							
Spin atomized	340	1.5–2.5	45	< 10	< 1.0	< 0.2	solid spheres
Vacuum atomized	110	2.5–3.0	250–310*	10–100	5–10	< 0.2	flakes, solid spheres†
Steam atomized	2000	1.5–5.0	200–1200	100–600	11–24	< 0.2	flakes, hollow spheres
Nickel base alloy IN-100							
Spin atomized	400	4.5–5.0	85	< 10	< 1.0	< 0.2	solid spheres
Vacuum atomized	300	5.0–7.5‡	50	—	5	< 0.2	flakes, solid spheres
Rotating electrode process atomized	170	~3.0	70	10	5.6	0.3	solid spheres
Argon atomized (fine powder)	75	~2.0	170	7	17	1.6	solid spheres with fine particles attached to coarser ones
Iron base alloy VM-300 Maraging steel							
Spin atomized	430	4.0–6.0	42	—	—	—	solid spheres
Vacuum atomized	300	6.0–7.0‡	53	10	5	< 0.2	flakes, solid spheres
Rotating electrode process atomized	180	2.0–3.0	40	—	5	< 0.2	solid spheres
Steam atomized	2000	4.5–11.0	150–2000	—	—	—	solid spheres with porosity
Argon atomized (coarse powder)§	2500	5.0–12.0	630	—	—	—	solid spheres with porosity

*Probably from retained slag.
†From [5].
§Further quenched in water tank.
‡Dendritic arm spacing values cover the size range 500 to 830 μm.

$$B = \frac{3h(T_M - T_0)}{R\rho_S H} \quad (3)$$

All the terms in Equations 2 and 3 are defined in the Appendix.

The combined radiation and convection heat-transfer coefficient in Equation 3 can be calculated using Equation A1 in the Appendix and data generated in Fig. 3. For example, for the Maraging 300 alloy, measured secondary dendrite arm spacing of a steam-atomized droplet, 1 mm in diameter, is ~ 6.5 μm. From Fig. 3 the corresponding cooling rate is 4×10^2 °C sec^{-1}. Using the values of heat capacity and density of Fe—25% Ni alloy* and an atomization temperature of 1500°C, the value of $h \simeq 3.9 \times 10^{-3}$ cal cm^{-2} sec^{-1} $°C^{-1}$ is calculated.

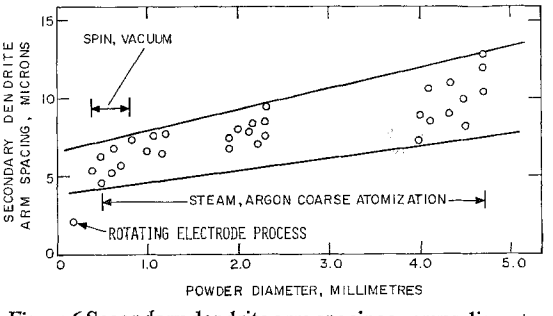

Figure 6 Secondary dendrite arm spacings versus diameter of spherical powders of Maraging 300 alloy produced by different atomization techniques.

Knowing the value of the heat-transfer coefficient permits prediction of solidification

*For Fe—25% Ni alloy, the following values have been reported [1, 2]: $C_p = 0.107$ cal g^{-1} $°C^{-1}$, $\rho = 8$ g cm^{-3}, and Latent heat of fusion, $H = 72$ cal g^{-1}.

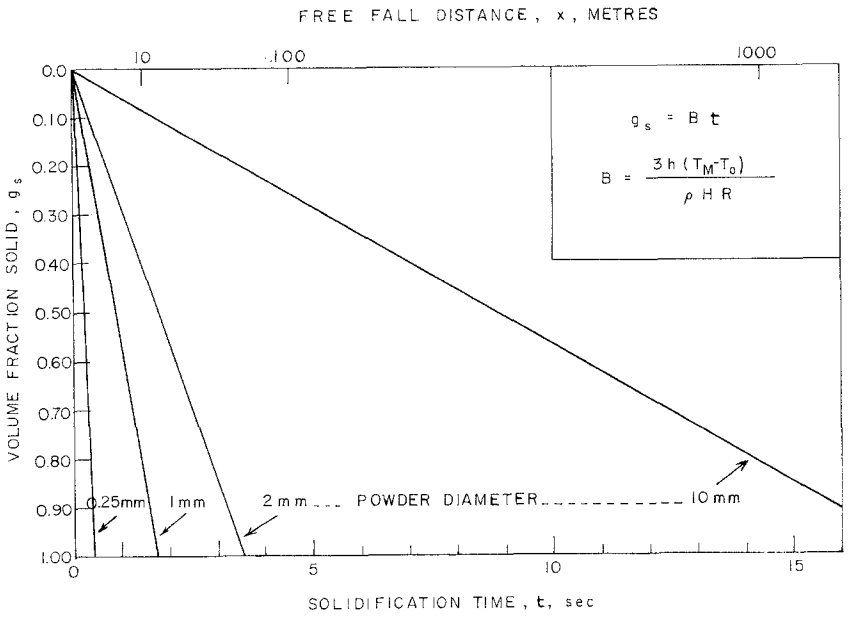

Figure 7 Calculated volume fraction solid versus solidification time and free fall distance for different size powder particles of Maraging 300 alloy.

time from Equations 2 and 3. Fig. 7 shows, for Maraging 300 alloy, calculated plots of volume fractions solidified versus solidification time for different size particles.

3.4. Structures of atomized droplets

During solidification of small atomized droplets, the rate of heat removal is "*h*-controlled"; only very small differences in temperature, and hence fractions solid, exist within each droplet. The corn-on-the-cob surface of the spin-atomized powder in Fig. 4b is due to existing liquid at the droplet surface feeding shrinkage near the end of solidification.

Examination of atomized powders of Maraging 300 alloy indicates that a substantial number of the liquid droplets were undercooled prior to nucleation of the solid. The microstructure of an undercooled droplet is shown in Fig. 8. The light etching in the centre of the dendrite arms is evidence of high solute cores signifying undercooled structures. This has previously been established by detailed optical examination and electron microprobe analysis of undercooled structures of Fe—25% Ni and Maraging 300 alloys [5, 7].

4. Conclusions

1. Pre-alloyed powders of Maraging 300, IN-100, and MAR-M-509 alloys were spheres and/or flakes of 75 to 2500 μm in average size, had oxygen contents of 40 to 2000 ppm and dendrite arm spacings of 1.5 to 12 μm, depending on the atomization process.

2. Rotating electrode process, spin- and vacuum-atomized powders have oxygen contents consistently less than 100 ppm. The first two are spherical in shape with relatively narrow size ranges. Vacuum-atomization, while lending itself to production of clean powders, gives little control over powder shape.

3. Secondary dendrite arm spacing in Maraging 300 alloy is proportional to local average cooling rate to an exponent of -0.30.

4. This empirical relationship between secondary dendrite arm spacings and cooling rates, coupled with a simple heat flow analysis, permits accurate estimates of heat-transfer coefficients and solidification times during atomization.

5. Cooling rates during atomization of Maraging 300 alloy by different processes are in the range of $\sim$ 54 to 2.1×10^4, with resulting dendrite arm spacings of $\sim$ 12 to 2 μm. Calculated heat-transfer coefficient for steam atomization of the alloy is 3.9×10^{-3} cal cm^{-2} sec^{-1} $°C^{-1}$.

6. Examination of atomized powders of

Maraging 300 alloy shows evidence of undercooling prior to nucleation of the solid.

Appendix: Heat flow during atomization

Newton's law of cooling for a small spherical droplet of radius R with "h-controlled" heat transfer is written:

$$q_{r=R} = 4\pi R^2 h(T - T_0) = 4/3\pi R^3 \rho C_p \frac{dT}{dt} \quad \text{(A1)}$$

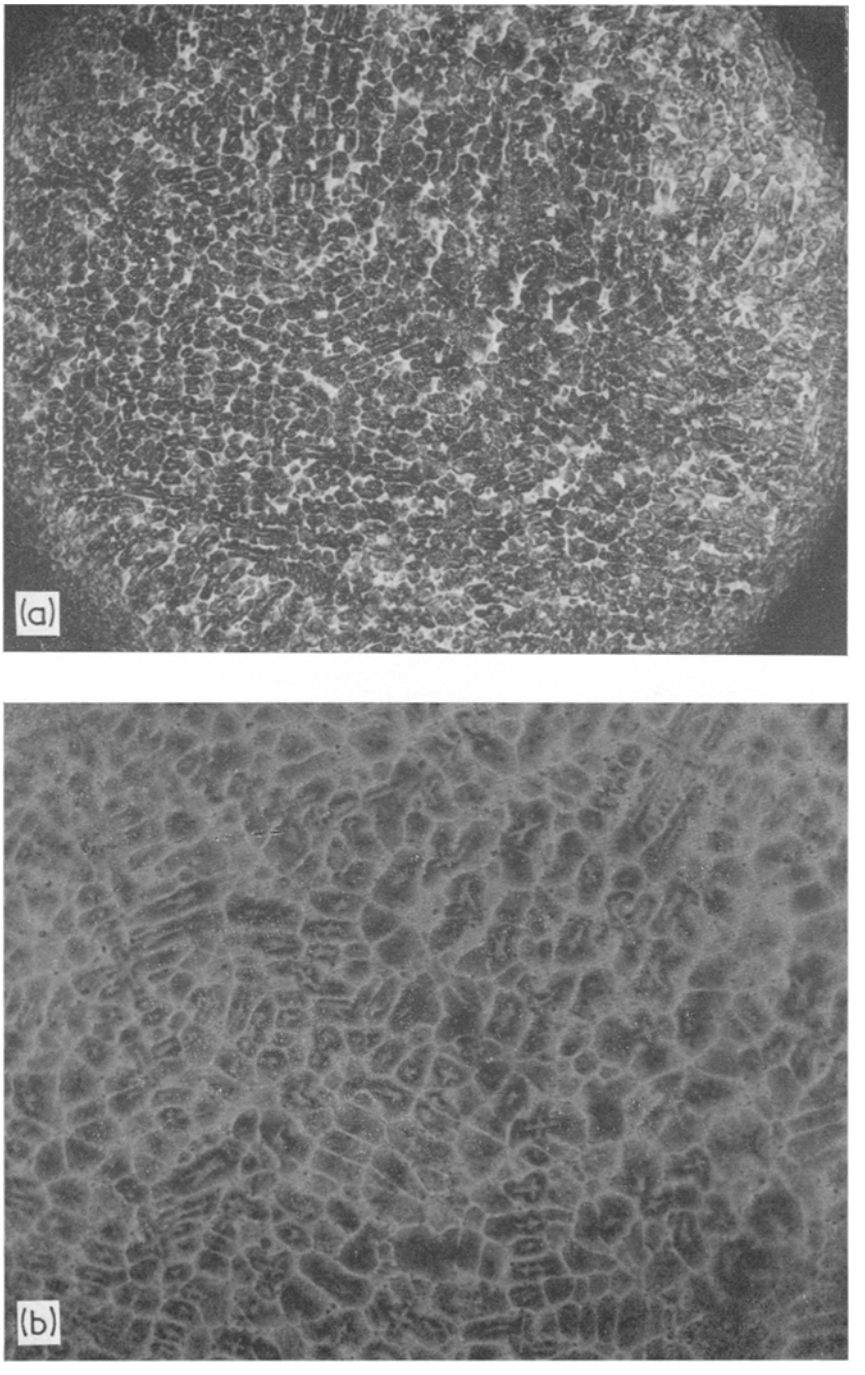

Figure 8 Photomicrographs of an undercooled powder particle of Maraging 300 alloy exhibiting high solute cores (light etching) in the dendrite arms; (a) × 200, (b) × 500.

where q = rate of heat flow at the droplet-coolant medium interface (cal sec^{-1}),
R = radius of the droplet (cm),
T = temperature of the droplet (°C),
T_0 = medium temperature (°C),
ρ = density of the alloy (g cm^{-3}),
C_p = specific heat of the alloy (cal g^{-1} $°C^{-1}$),
h = heat-transfer coefficient, *radiation plus convection* (cal cm^{-2} sec^{-1} $°C^{-1}$),
$dT/dt = \epsilon$ = cooling rate at temperature T (°C sec^{-1}).

Assuming that the rate of heat extraction during solidification is the same as during cooling of the droplet prior to solidification, the following heat balance can be established:

$$\frac{3}{R} h(T_M - T_0) = C_p \rho \frac{dT}{dt} = \rho_s H \frac{dg_s}{dt} \qquad (A2)$$

where g_s = volume fraction solidified,
T_M = melting temperature of the droplet (°C),
H = latent heat of fusion (cal g^{-1}).

Equation A2 further assumes that the size of the "mushy" zone in the alloy is small enough that solidification essentially takes place at a single temperature. With initial boundary conditions of $g_s = 0$ at $t = 0$, Equation A2 is integrated to obtain

$$g_s = Bt \qquad (A3)$$

where

$$B = \frac{3h(T_M - T_0)}{R\rho_s H}. \qquad (A4)$$

For complete solidification of the droplet, $g_s = 1.0$ and $t_f = 1/B$.

Acknowledgement

The work reported here was conducted under the sponsorship of the Advanced Research Projects Agency. The authors would like to express their appreciation to Drs Peter E. Price and Robert Widmer of Industrial Materials Technology, and to Dr Robert Cunningham of Chemstrand Research Center for supplying some of the powders used in this study.

References

1. W. E. BROWER, JUN, R. STRACHAN and M. C. FLEMINGS, *Cast Metals Research J.* **6** (4) (1970) 176.
2. W. E. BROWER, JUN, "Solidification Structure Fracture Relations in Inclusion Bearing Iron", Ph.D. Thesis, Department of Metallurgy and Materials Science, Massachusetts Institute of Technology (1969).
3. T. F. BOWER, H. D. BRODY and M. C. FLEMINGS, *Trans. Met. Soc. AIME* **236** (1966) 624.
4. M. C. FLEMINGS, D. R. POIRER, R. V. BARONE and H. D. BRODY, *J.I.S.I.* **208** (1970) 371.
5. R. K. ROBINSON, "Development of P/M Cobalt-Base Alloys Using Rapidly Quenched, Pre-Alloyed Powders", Sc.D. Thesis, Department of Metallurgy and Materials Science, Massachusetts Institute of Technology (1973).
6. T. Z. KATTAMIS, *Met. Trans.* **2** (1971) 2000.
7. T. Z. KATTAMIS and R. MEHRABIAN, to be published in *J. Mater. Sci.*

Received 7 February and accepted 27 February 1974.